

Seismic image enhancement in post stack depth migration by finite offset CDS stack method

Mehrdad Soleimani¹ · Morteza Balarostaghi¹

Received: 19 December 2014 / Accepted: 9 February 2016 / Published online: 25 February 2016
© The Author(s) 2016. This article is published with open access at Springerlink.com

Abstract Seismic imaging in complex geological structures such as thrust belts and areas with complex geological structures is affected by several factors that often lead to poor-quality final result. Usually such structures produce locally very steep dips, strong lateral variations in velocity and abrupt truncation of the reflectors. Common reflection surface stack is a macro velocity model independent method that is introduced for seismic imaging in complex media. However, this method has some drawbacks in imaging of low-quality data from complex structures. Many improvements to this method have been introduced in several researches to overcome this drawback. However, the problem of conflicting dips situation is still a problematic issue in this method. In this study, a new method, called finite offset common diffraction surface (FO-CDS) stack, is introduced to overcome this problem and remove some geological interpretation ambiguities in seismic sections. This method is based on improving the CDS stack operator, with the idea of partial common reflection surface stack. This modification will enhance the quality of the final seismic image, where it suffers from conflicting dips problem and low signal to noise ratio. The new idea is to change the operator of the CDS equation into a finite offset mode in different steps for each sample. Subsequently, a time-variant linear function is designed for each sample to define the offset range using FO-CDS operator. The width

of this function is designed according to the Fresnel zone. The new operator was applied on a synthetic and a real low fold land data. Results show the ability of the new method in enhancing the quality of the stacked section in the presence of faults and conflicting dips.

Keywords Seismic imaging · Complex structures · Common reflection surface · Diffraction surface · Finite offset

Introduction

Seismic imaging generally relies on data quality, velocity reliability, and migration operator performance. The standard imaging methods, which are based on the Kirchhoff integral, have both theoretical and practical shortcomings in resolving some of the imaging problems. Most of the problems in seismic imaging of geological settings are due to the complexities in structure and rock types. The term ‘complex’ is used for those geological settings which cannot be easily imaged. Therefore, in the past few years substantial efforts have been spent in developing new imaging methods.

Some data-driven imaging techniques are introduced to simulate zero offset (ZO) sections from multi-coverage seismic reflection data. Some of these methods are polystack (de Bazelaire 1988), multi-focusing (MF) (Gelchinsky et al. 1999a, b), the common-reflection-surface (CRS) (Hubral 1999), and 3-D angle gathers (Fomel 2011) techniques. Figure 1 shows the classification of seismic imaging methods.

These methods are data driven in the way that they use a multiparameter moveout formulas, where the moveout parameters are derived based on coherency analysis. They also do not make use of an explicit macro velocity model.

✉ Mehrdad Soleimani
mehrdad_soleimani2005@yahoo.co.nz;
msoleimani@shahroodut.ac.ir

Morteza Balarostaghi
balarostaghi@shahroodut.ac.ir

¹ Faculty of Mining, Petroleum and Geophysics, University of Shahrood, No. 37, Shahrood, Iran

Fig. 1 Classification of seismic imaging methods, (Sava and Hill 2009)

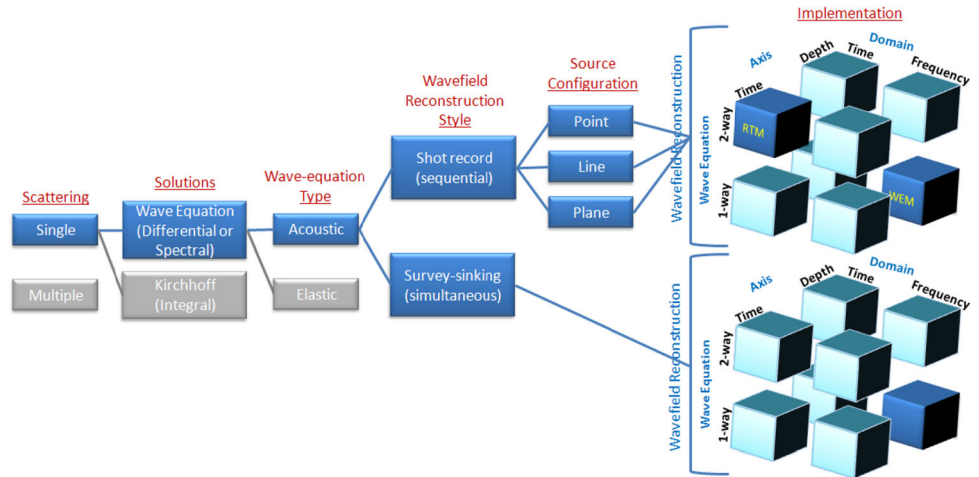
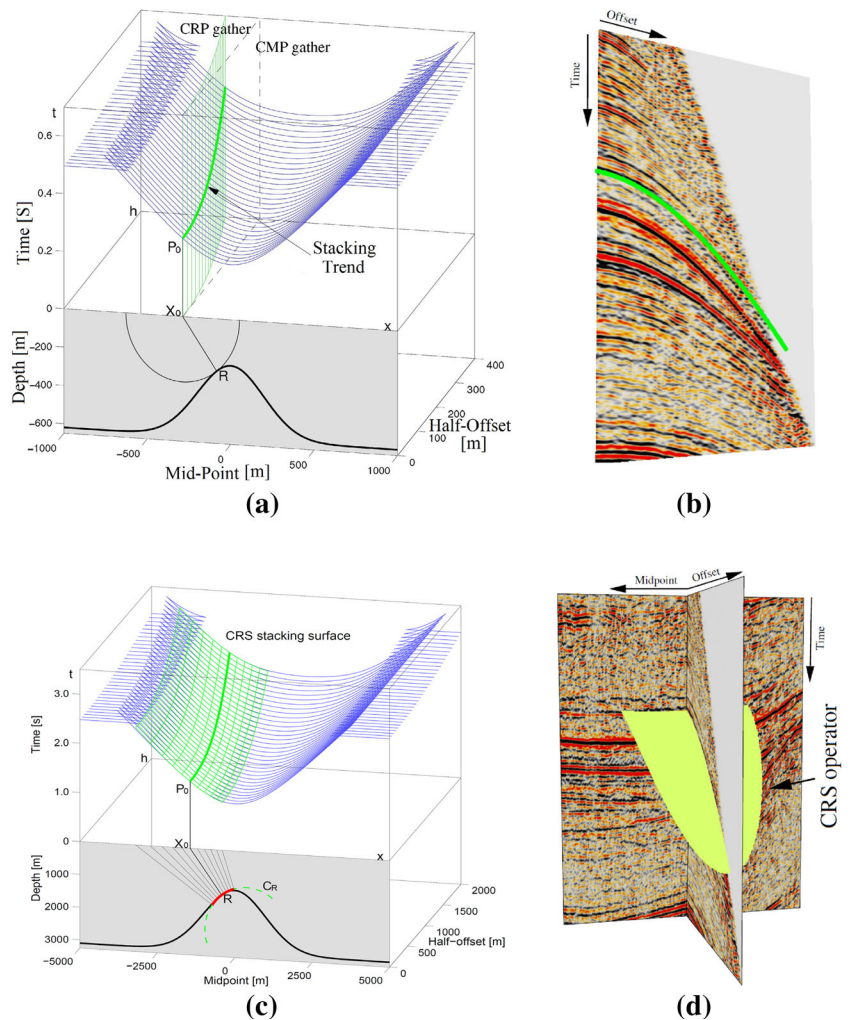


Fig. 2 a A homogenous anticline model in depth domain with its related common *offset curves* (in blue) in (t, x, h) domain, showing the CRP trend and the CMP gather (green) related to point R in depth. **b** The related CRP stacking trend in a real seismic CMP gather. **c** The CRS stacking operator (green) in (t, x, h) domain related to red line on the reflector in depth. **d** The related CRS operator on real seismic data. [a Müller (1999), b Bergler (2001), c Hertweck et al. (2007), and d Mann et al. (2007)]



The CRS stack multiparameter moveout equation in time—midpoint—half offset (t, x, h) domain describes a stacking surface rather than a trend in the conventional common midpoint (CMP) stack (Hertweck et al. 2007)

(Fig. 2). Due to this improvement in stacking strategy, the CRS method has been also used to increase the signal to noise ratio in 3D seismic imaging of faulted complex structure (Buness et al. 2014). However, the CRS stack

suffers from the problem of conflicting dips. Several researches have been performed to resolve this problem in the literature of the CRS.

Soleimani et al. (2009b) introduced a CRS modification, called data-driven common diffraction surface (CDS) stack or data based CDS stack method.

Baykulov (2009) used a multiparameter CRS traveltime equation which tries to improve the quality of prestack seismic reflection data in a process called partial CRS stack. The advantage of the partial CRS stack algorithm is that it is robust and easy to implement. Like the conventional CRS, the partial CRS stack also uses information about local dip and curvature of each reflector element. Due to the constructive summation of coherent events, the partial CRS stack enhances the signal and attenuates random noise (Baykulov 2009). Similar to the CRS stack method, the partial CRS stack takes the information from conflicting dips into account. However, they both approach the problem of conflicting dips in a different way that the data-based CDS stack does.

Shahsavani et al. (2011) introduced the model-based CDS stack method that decreases the large computation time of the previous data-driven CDS stack. However, it was based on a predefined velocity model that makes it a velocity model-dependent approach.

Garabito et al. (2011) introduced the surface operator of the CDS method that was a special case of the data-driven CDS, when only the dominant surface is considered as the final stacking operator. Yang et al. (2012) called the situation caused by conflicting dip problems as dip discrimination phenomenon and handled this problem with migration/de-migration approach. Schwarz et al. (2014) introduced the implicit CRS that combines the robustness of the CRS, regarding heterogeneities with the high sensitivity to curvature of the MF approach. However, it assumes reflectors to be locally circular that might not be a good idea for precise imaging of reflection truncation.

Conflicting dips problem in the crs

The CRS stack is a multi-parameter stacking method that uses any contribution along any realization of its operator. These contributions are tested by coherence analysis for each ZO sample, and the set of attributes, which yield the highest coherency, is accepted as the optimum operator parameters to perform the actual stack (Höcht et al. 2009). Figure 2c, shows the green CRS stack operator compared to the conventional CMP stack in Fig. 2a. The CRS stack method has the potential to sum up more coherent energy from the data that result in high signal-to-noise ratio in the simulated ZO section (Mann et al. 1999).

The CRS equation is described by three parameters α , R_N , and R_{NIP} , (known as kinematic wavefield attributes) instead of one parameter for classical CMP stack (Mann 2002).

The CRS equation with its three attributes in hyperbolic and parabolic forms reads (Müller 1998)

$$t_{\text{hyperbolic}}^2(x_m, h) = \left[t_0 + \frac{2 \sin \alpha (x_m - x_0)}{v_0} \right]^2 + \frac{2t_0 \cos^2 \alpha}{v_0} \times \left[\frac{(x_m - x_0)^2}{R_N} + \frac{h^2}{R_{NIP}} \right] \quad (1)$$

$$t_{\text{parabolic}}(x_m, h) = \left[t_0 + \frac{2 \sin \alpha (x_m - x_0)}{v_0} \right] + \frac{\cos^2 \alpha}{v_0} \left[\frac{(x_m - x_0)^2}{R_N} + \frac{h^2}{R_{NIP}} \right], \quad (2)$$

where h is the half-offset, $(x_m - x_0)$ is the midpoint displacement with respect to the considered CMP position, and t_0 corresponds to the zero offset (ZO) two-way traveltime (TWT). The emergence angle of the ZO ray is shown by α , the radius of curvature of the normal (N) wave by R_N , the radius of the normal incidence point (NIP) wave by R_{NIP} , and V_0 is the near-surface velocity.

These attributes are shown in Fig. 3. By these attributes, the curvature, dip, and depth of the reflector in the considered element shown by red line in Fig. 2c are defined. Figure 3b shows the radius of the NIP wave.

The CRS stack method assigns merely one optimum stacking operator for each zero offset (ZO) sample to be simulated (Heilmann 2007). However, in the situation where different events in a seismic section intersect each other and/or themselves, only a single stacking operator for each ZO sample would not be appropriate. Thus, Mann (2001) proposed to allow small discrete number of stacking operators for a particular ZO sample. Therefore, in conflicting dip situations, more than one operator for each ZO sample in the ZO stack simulation would be used, called the extended search strategy method in the CRS. However, the extended search strategy and partial CRS stack do not guarantee that all the weak diffraction events appear in the final stacked section.

Data-driven cds stack method

The data-driven CDS stack method was introduced to resolve the conflicting dips problem and to enhance more weak diffraction events that might get lost in the other modification of the CRS method. This method, which was introduced by Soleimani et al. (2009b), brings the idea of dip move-out (DMO) from conventional processing methods into the CRS method.

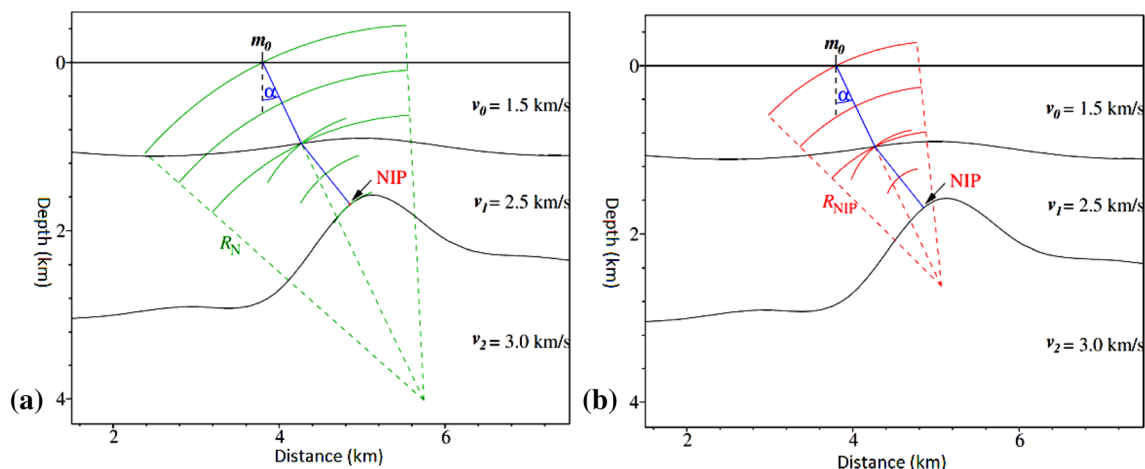


Fig. 3 Three kinematic wavefield attributes. **a** The central ray and the emergence angle, α , shown by blue line and the radius of normal wave, R_N . **b** Radius of the normal incidence point wave, R_{NIP} . Spinner (2007)

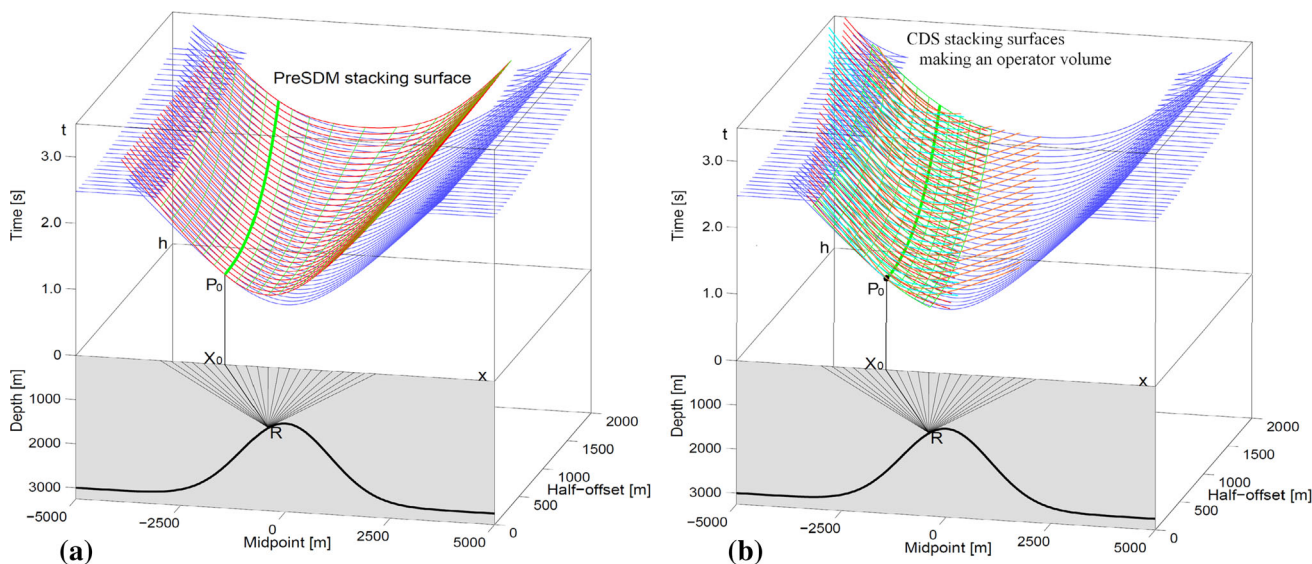


Fig. 4 **a** Shape of the CRS operator corresponding to a curved reflector segment in depth; **b** shape of the CDS operators corresponding to the same diffraction point, [**a** from Heilmann (2007) and **b** from Soleimani et al. (2009b)]

Figure 4a shows the stacking surface of a pre-stack depth migration (PSDM) operator. This surface considers point R on the reflector as a diffraction point. In pre-stack migration, data are summed along the red surface that is the kinematic response of a diffractor point at R. A PSDM operator can also be described by the thin green CRP trajectories related to hypothetical reflectors of different dips in Fig. 4a. If constructed for each point in the (x_m, z) plane, in which subsurface reflector or diffractor images are searched for, one can perform stacking along all PSDM operators. In the context of PSDM, a reflector can consequently be conceived as a superposition of diffraction points. In the data-driven CDS stack method, same idea of diffraction point is used and applied only for more than one

surface. Therefore many stacking surfaces for one sample in the (t, x_m, h) domain is produced that makes a volume of stacking operators, where all these operators contribute into stacking (Fig. 4b). Thus, the conflicting dips will be treated well by the CDS stack operator.

Finally, stacking performs in these surfaces (Fig. 4b) and the (optionally weighted) result of each stacking is allocated to the ZO sample, here P_0 . Resolving the problem of conflicting dips in this way will enhance all weak diffraction events in the stacked section (Soleimani et al. 2009a). For true diffraction events, the radii of the NIP wave and normal wave coincide, $R_N = R_{NIP}$. Thus, the only attribute to be searched for in a specific emergence angle is a combination of R_N and R_{NIP} that is called R_{CDS} .

Therefore, the travel time Eq. (1) converts to the CDS travel time approximation as (Soleimani et al. 2009b) follows:

$$t^2(x_m h) = \left(t_0 + \frac{2 \sin \alpha}{v_0} (x_m - x_0) \right)^2 + \frac{2 t_0 \cos^2 \alpha}{v_0 R_{CDS}} \times \left((x_m - x_0)^2 + h^2 \right) \quad (3)$$

By implicit knowledge of the R_{CDS} , the shape of the operator could be easily defined. However, the data-driven CDS stack approach is time-consuming due to separate stacking operator definition for each angle.

Finite offset CDS stack method

To better resolve the problem of conflicting dips, here we used the idea of the partial CRS stack (Fig. 5a) to modify the data-driven CDS stack into the finite offset data-driven CDS stack, (FO-CDS). The FO-CDS uses the idea of partitioning the stacking surfaces shown in Fig. 5b. The FO-CDS stack method calculates collection of stacking surfaces around a specified point. The summation result is assigned to that sample, here P_0 . The operator equation in FO-CDS is the same as CDS operator with performing limitation in offset range according to an offset banding function. In Eq. (3), the offset is limited by this condition:

$$b t_0 + c < h < b t_0 + d \text{ and } dh = d - c, \quad (4)$$

where dh is the length of offset range; b , c , and d are constant values for defining the offset banding length and

increment. Parameter b controls the variation of the offset rang versus time or depth of the reflectors. Parameters c and d control the optimum magnitude and position of the offset range for each t_0 . Parameter $d - c$ determines the length of the offset range in this method.

Figure 6 depicts the offset banding function for 2D FO-CDS stack method. Parameters a , b , c , and d should be defined by analyzing different values. The simplified strategy to perform the finite offset CDS stack is shown in Fig. 7.

Aperture and offset banding function definition

The intersection of the Fresnel volume with a reflecting interface defines the so-called Fresnel zone which is the natural limit of resolution (Fig. 8). Obviously, the interface of Fresnel zone is a frequency-dependent parameter, such that waves with higher frequency provide higher spatial resolution.

For monochromatic signals with period T , the interface Fresnel zone consists of all points, M , on the interface for which the following inequality holds (Cerveny and Soares 1992):

$$|t(S, M, R) - t(S, \bar{M}) - t(\bar{M}, R)| \leq T/2 \quad (5)$$

The complete set of the CRS wavefield attributes allows estimating the size of the projected first Fresnel zone. This can be done by comparing the traveltimes of the actual reflection event with the traveltimes of its associated diffraction event ($R_{NIP} = R_N$). The locations where these

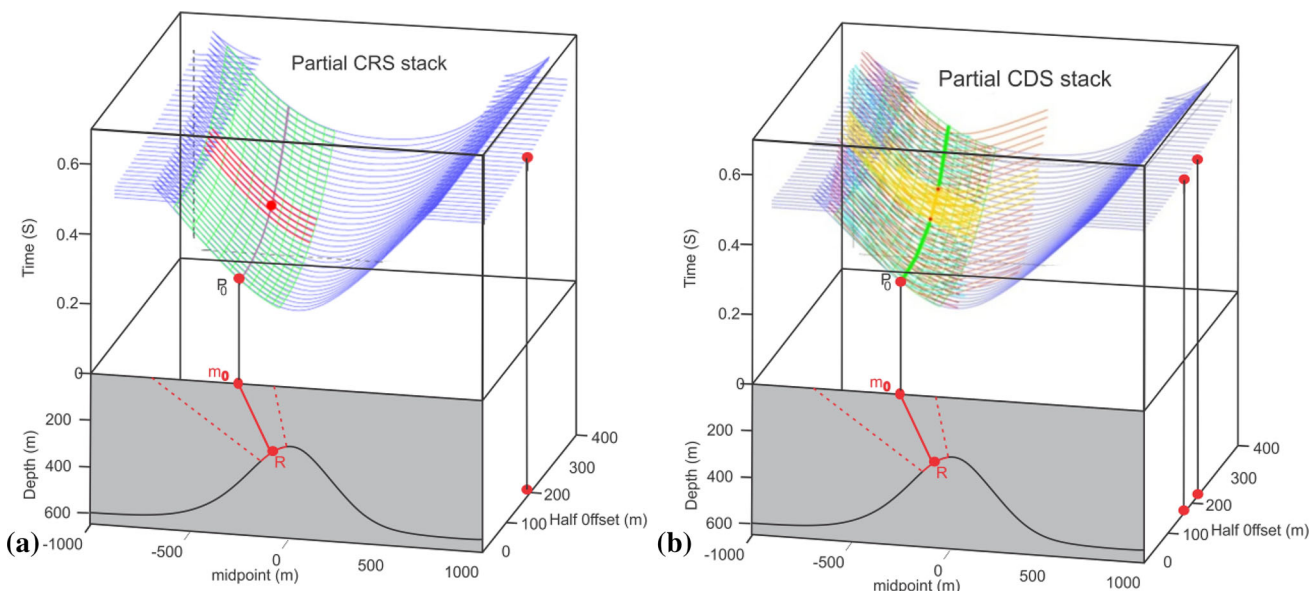


Fig. 5 a The partial CRS stack performs summation of data around the specified point on a CMP traveltime curve (magenta line) and assigns the result to the same point in a newly generated CRS

supergather. **b** The finite offset CDS stacking surface shown with a yellow color coincides locally with the CDS stacking surface (red color), but may be limited in size. [a from Baykulov (2009)]

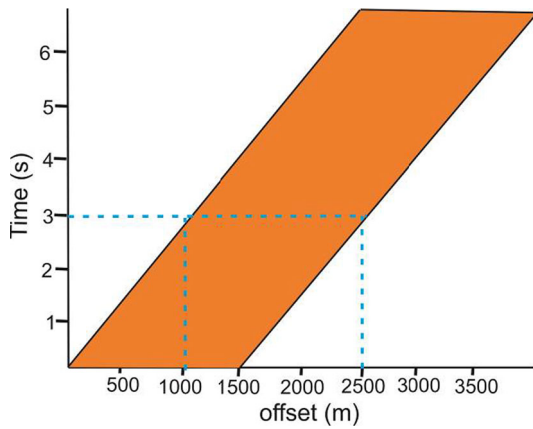


Fig. 6 Offset banding function that defines the offset range for each sample

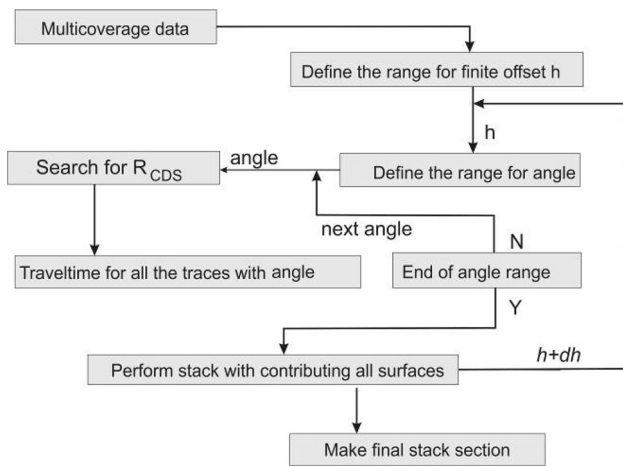


Fig. 7 Simplified flowchart of the finite-offset CDS stack search strategy

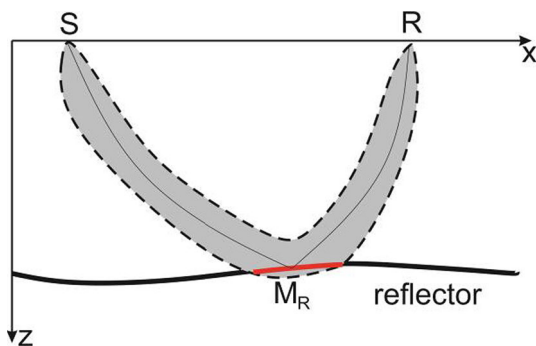


Fig. 8 Schematic sketch of the Fresnel zone (gray) of a reflected ray $SM_R R$. The intersection of the Fresnel volume with a reflecting interface defines the interface Fresnel zone (red), Spinner (2007)

events differ by half of the temporal wavelet length define the extension of the projected first Fresnel zone, and thus, the optimum aperture. Obviously, the projected Fresnel zone size is readily defined for each attribute set to be

tested. The half-width of the projected Fresnel zone reads (Mann 2002) as follows:

$$|t_{par}^{Ref} - t_{par}^{Dif}| = \frac{W_F}{2} = \frac{1}{\cos \alpha} \sqrt{\frac{v_0 T}{2 \left| \frac{1}{R_N} - \frac{1}{R_{NIP}} \right|}}, \quad (6)$$

where W_F is the width of the Fresnel zone, t_{par}^{Ref} is the reflection parabolic travel time, t_{par}^{Dif} is the parabolic diffraction travel time, v_0 is the surface velocity, and α , R_N , and R_{NIP} are the CRS attributes. Equation (6) is derived from the parabolic traveltimes approximation (Eq. 2) instead of the hyperbolic approximation (Eq. 1). The parabolic representation leads to a simpler formula with a projected Fresnel zone, symmetric to the midpoint under consideration (Mann 2002). However, estimation from parabolic traveltimes equation does not affect the final result. It is only selected due to its simplicity and will result to a same value if the hyperbolic approximation is used. But it is not the case for stacking operator definition.

Aperture shape in the FO-CDS method is defined as in the CRS. However, in the FO-CDS the aperture is defined according to Eq. (6). The aperture shape is shown in Fig. 9.

Synthetic data example

Sigsbee 2A synthetic data are a constant density acoustic synthetic dataset that consists of a salt body with very complex geometrical characteristics. In this study, we used only the faulted part of the data, the same part used by Mann (2002) and Baykulov (2009) (Fig. 10). To show advantages of applying the FO-CDS stack method to a noisy data, Gaussian noise with $S/N = 20$ was added to the synthetic seismic data. The extended search strategy results of Mann (2002) and partial CRS stack of Baykulov (2009) were also used for comparison. Figure 11 shows the results of the data-driven CDS, FO-CDS, extended search CRS, and partial CRS stack methods. The stacking process by finite offset method makes better continuity of reflections and resolves more efficiently the problem of conflicting dips rather than considering all offset ranges in the data-driven CDS stack methods. The extended search strategy and partial CRS stack method could also resolve the problem of conflicting dips, where more diffraction events obviously are imaged by the FO-CDS stack method.

Real land data example

The Gorgan region is located in the North East of Iran, east of the Caspian Sea. In most seismic surveys in this area, the mud volcanoes play an important role for planning the seismic surveying line. Mud volcanoes not only increase

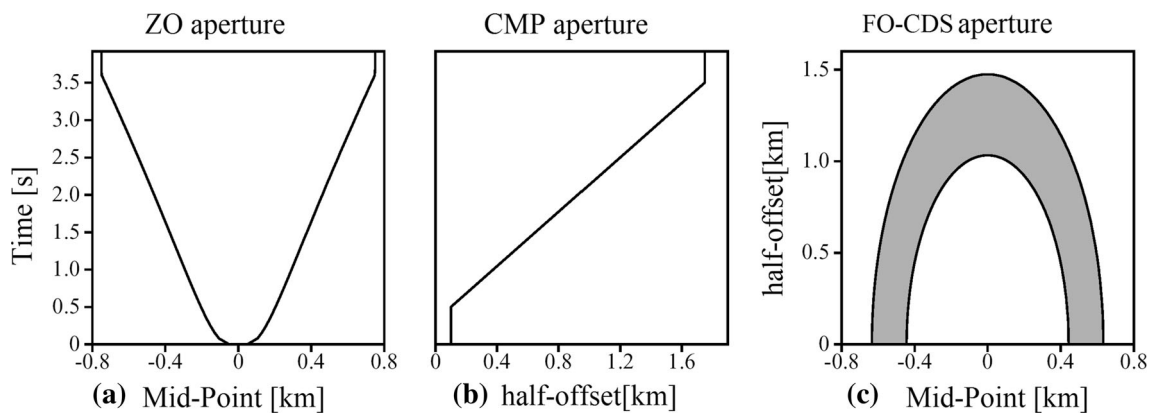


Fig. 9 Shape of the aperture in the FO-CDS that is like as the CRS aperture, but different in size according to the Fresnel zone

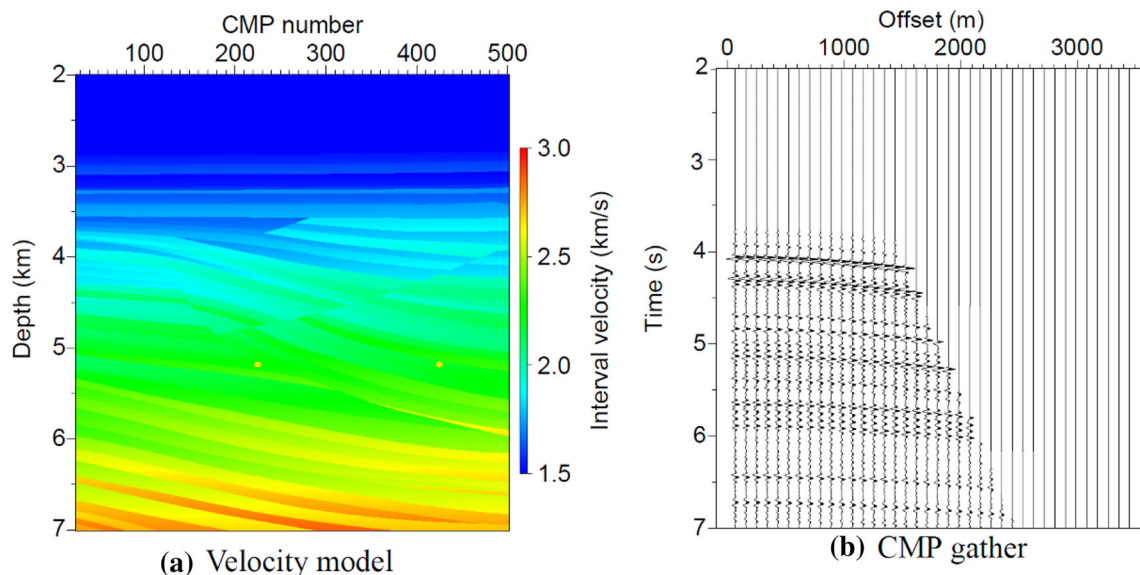


Fig. 10 Sigbee 2A model and data: True interval velocity model (a) and a CMP gather (b). Fluctuations of interval velocities of up to ± 100 m/s from the gradient model produce the reflections in the CMP gather

complexity of the geological condition, but also reduce the *S/N* ratio of the data due to strong absorption coefficient of mud. The FO-CDS and the CDS stack methods were applied on a real 2D data from this region. A raw CDP gather of the data is shown in Fig. 12a.

As could be seen, seismic data suffer from different linear noises, air blast noise, ground roll, and random noise in large amounts. As mentioned earlier, the CDS and the FO-CDS stack methods enhance any weak diffraction events existing in the pre-stack data. Therefore, in such a data with lots of coherent and non-coherent noises, care should be taken to suppress them as much as possible in pre-processing steps. Figure 12b shows the same CDP gather after strong noise attenuation. Then after, the CDS and the FO-CDS stack methods were applied on the pre-stack data. Table 1, shows parameters used for the CDS

and the FO-CDS processing. Figure 13 shows the result of the data-driven CDS and the FO-CDS stack methods. As could be seen, the reflection events, especially the horizontal events in the top part of the sections, are well imaged in both methods. The improved parts are shown by rectangles and circles in Fig. 13b. It should be noted that excessive mud in this region absorbs the seismic energy passing through the subsurface layers. It also disturbs the ray path which makes the quality of the stacked section, dramatically poor.

However, enhancing weak diffraction events related to the body of mud volcano guarantee defining the geological structure in post stack imaging. Here is where the greatest advantage of the FO-CDS stack methods appears. The FO-CDS stack method provides a super input for further imaging. Consequently, the CDS and the FO-CDS stacked

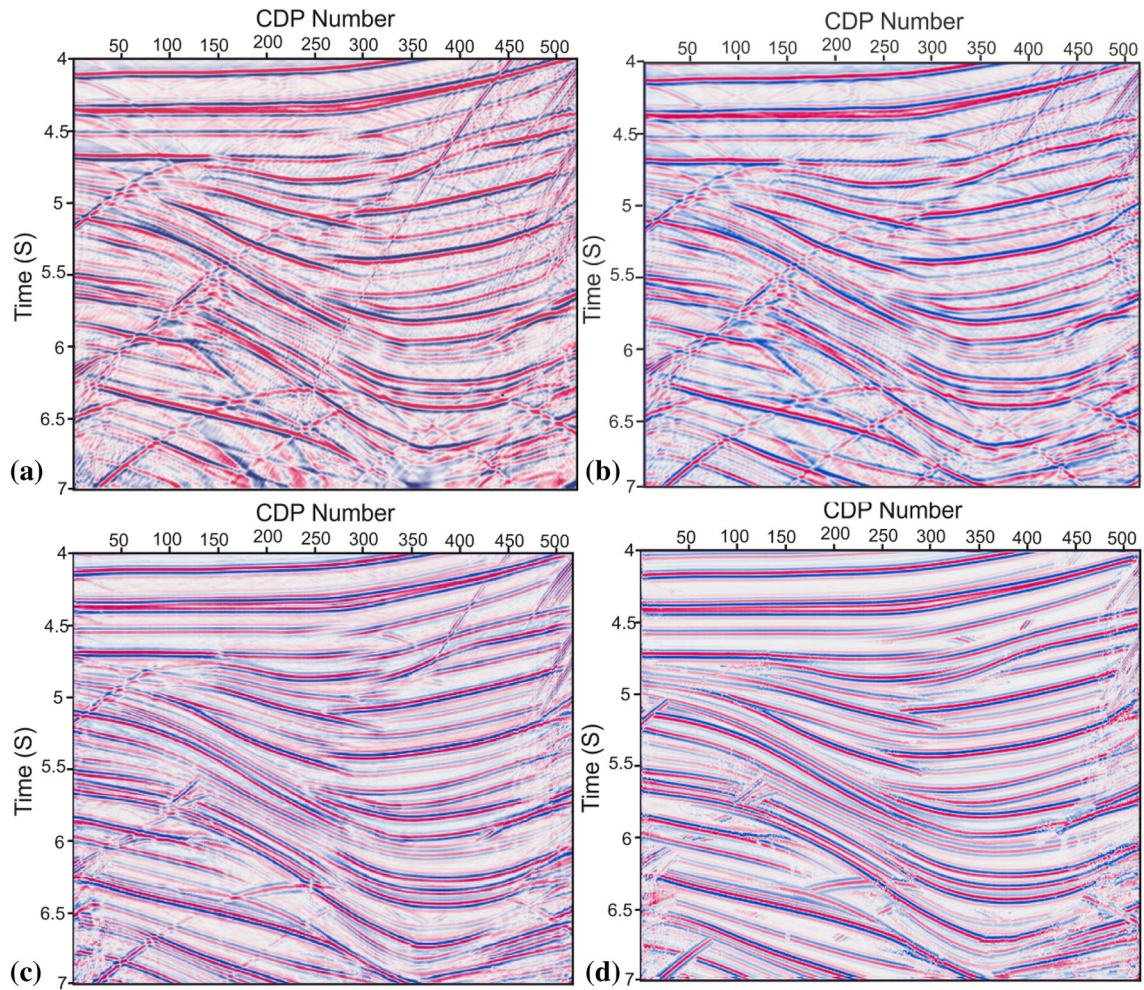


Fig. 11 **a** Stacked section obtained by the FO-CDS stack operator and **b** stacked section obtained by the data-driven CDS stack. **c** The partial CRS stack result and **d** the result of the extended search

strategy of the CRS. In the FO-CDS stacked section, weaker diffraction events are imaged in the stacked section

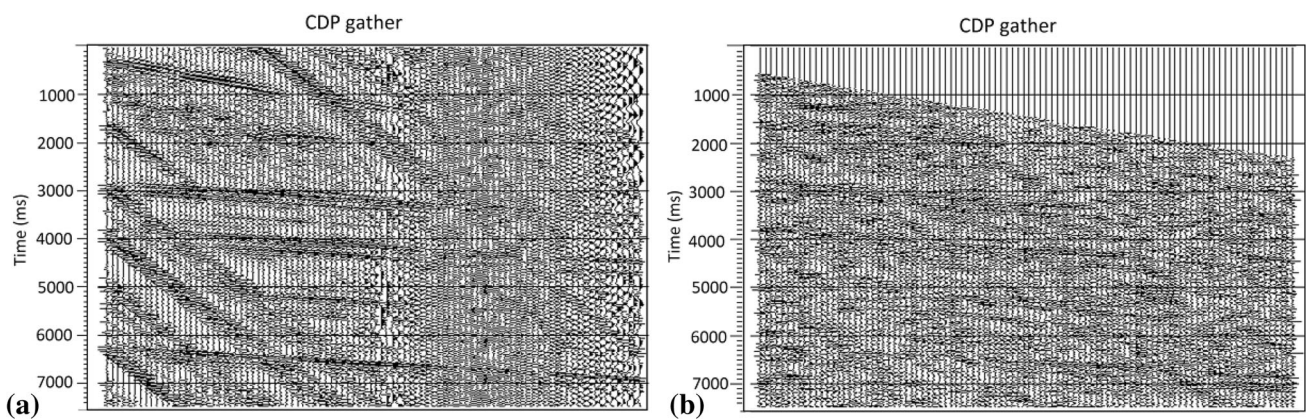
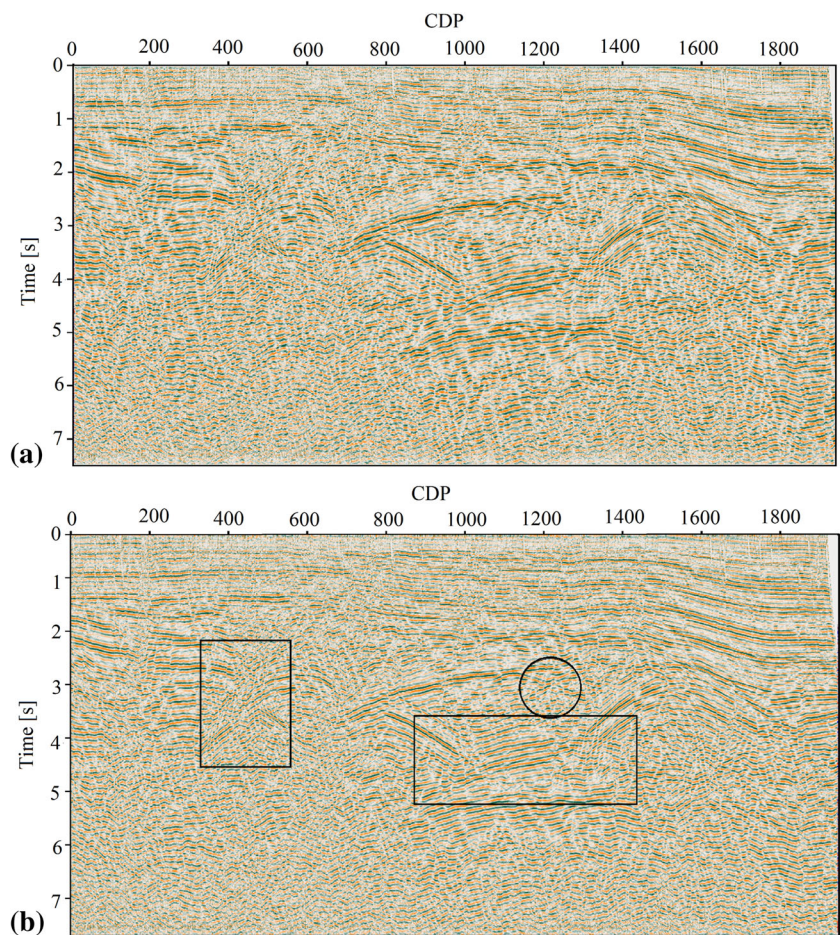


Fig. 12 The CDP gathers of the real data **a** before noise attenuation and **b** after pre-processing steps; data ready for the CRS and the FO-CDS stacking methods

Table 1 Processing parameters for the CDS and the FO-CDS stack of the real data

Context	Processing parameters	Setting
General parameters	Dominant frequency	30 Hz
	Coherence measure	Semblance
	Data used for coherence analysis	Original traces
	Temporal width of coherence band	56 ms
Velocity and constraints	Near-surface velocity	1300 m/s
	Tested stacking velocity	1300–4300 m/s
Target zone	Simulated ZO traveltimes for left part	0–7 s
	Simulated temporal sampling intervals	4 ms
	Number of simulated stacked traces	2010
	Spacing of simulated stacked traces	12.5 m
FO-CDS parameter	Tested emergence angle	−60° to +60°
	Initial emergence angle increment	1°
	Factor of CS search sampling rate	2 ms
	Number of iterations in CS search	3
	Process termination time for the FO CDS stack	11.15 h, (real time)
Hardware used	Super micro server used 10 CPUs server with 80 Gb RAM for processing	

Fig. 13 **a** The CDS stacked section and **b** the FO-CDS stacked section



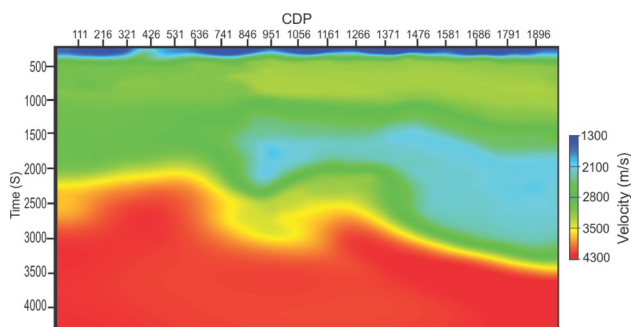


Fig. 14 The velocity model used for post stack depth migration

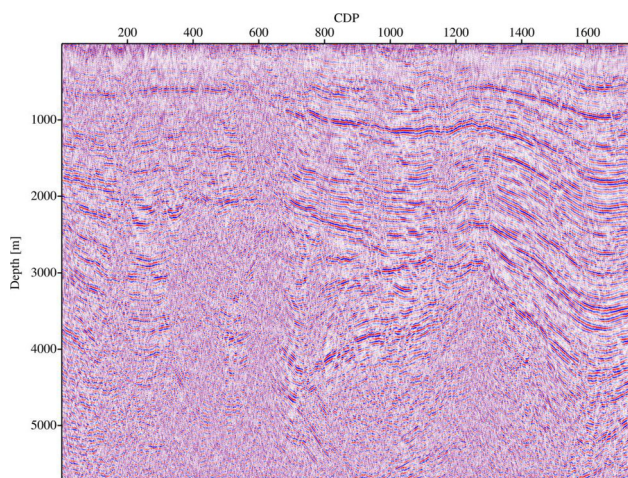


Fig. 15 Post SDM of the CDS stacked section. Reflectors are continuous in the *upper layers*

sections were used as input for the post stack Kirchhoff depth imaging.

The migration velocity model obtained by the NIP tomography method which was introduced by Duveneck (2004). The velocity model is shown in Fig. 14. The migration result performed on the data-driven CDS stacked section is shown in Fig. 15. The section shows a layered media in top (from the surface to the depth of 2000 m in left and 4000 m in right).

Figure 16 shows the result of migration on the FO-CDS stacked section. In the first glance, the improvement in signal-to-noise ratio and especially in the horizontal resolution is noticeable. The FO-CDS stack operator brought more energy in the stacked section that might not be taken into account by other methods. Therefore, more events with more details are imaged in the final migrated section. Boundaries of mud volcanoes can be drawn better, and faults in the upper right of the section are also imaged well.

The reflectors and other geological structures produced diffraction events that can be seen clearly here in this

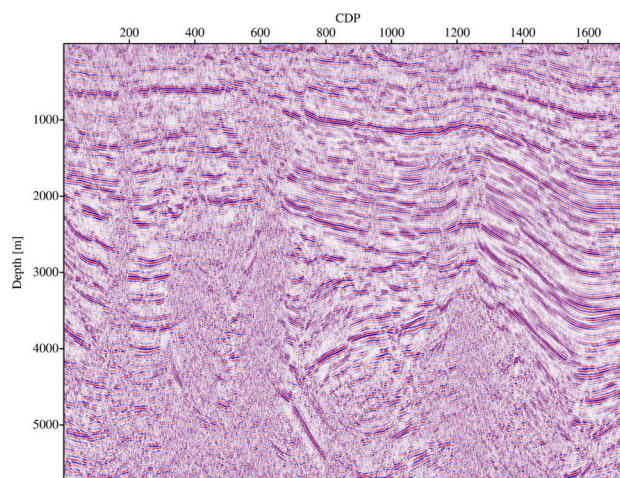


Fig. 16 Post SDM of the FO-CDS stacked section

section. Wedges between CDPs 800 and 1100 below the unconformity are imaged well, too. These wedges were clearly imaged by migration of the FO-CDS stacked section.

The result could be compared with the Ridgelet transform, which uses the Radon transform. However, the Ridgelet transform produces adverse effects on the inclined features and curved features when seismic data are reconstructed back from their filter coefficients (Sajid and Ghosh 2014).

Finally, we could say that migration on the FO-CDS stacked section focuses the energy of diffraction events in their apexes. Therefore, it not only shows the truncation of the reflectors at the body of the mud volcanoes, but also better shows their upper boundary. Thus, it could be concluded that the post stack depth migration of the FO-CDS stack method can be applied to complex structures to resolve some of the ambiguities of imaging in complex structures.

Conclusion

The finite offset CDS stack method was introduced here to resolve some of the seismic imaging problems in complex geological structures. The result of the FO-CDS stack followed by depth migration showed that it can serve as a suitable method for that purpose. This mainly relates to the stacking operator that gathers most of the energy of a selected ZO sample that existed in the pre-stack data. The FO-CDS operator enhances weak diffraction events which would be covered by dominant reflections in other methods. These events are mostly diffractions that are related to structures such as faults or mud volcano body. The FO-CDS stack method was applied on two synthetic and real

data sets. After conventional pre-processing, the data set was processed by the CDS and FO-CDS stack methods. The velocity model was built by NIP tomography technique and then used for post stack depth migration. The migrated sections showed that the FO-CDS method can clearly define the body of mud volcanoes that was not imaged well by other methods. The near-surface faults and the larger fault that was continued to larger times were also imaged better in the migrated section of the FO-CDS stacked result. Therefore, it could be concluded that the FO-CDS operator provides suitable stacked section for further imaging in complex media.

Open Access This article is distributed under the terms of the Creative Commons Attribution 4.0 International License (<http://creativecommons.org/licenses/by/4.0/>), which permits unrestricted use, distribution, and reproduction in any medium, provided you give appropriate credit to the original author(s) and the source, provide a link to the Creative Commons license, and indicate if changes were made.

References

- Baykulov M (2009) Seismic imaging in complex media with the common reflection surface stack. Ph.D. thesis, Hamburg University, Hamburg, p 129
- Bergler S (2001) The common reflection surface stack for common offset, theory and application. MSc. thesis, University of Karlsruhe, Karlsruhe, p 93
- Buness HA, Hartmann HV, Rumpel HM, Kraeczyk CM, Schulz R (2014) Fault imaging in sparsely sampled 3D seismic data using common-reflection-surface processing and attribute analysis—a study in the Upper Rhine Graben. *Geophys Prospect* 62(3):443–452
- Cervený V, Soares J (1992) Fresnel volume ray tracing. *Geophysics* 57:902–915
- de Bazelaire E (1988) Normal moveout revisited: inhomogeneous media and curved interfaces. *Geophysics* 53:143–157
- Duveneck E (2004) Velocity model estimation with data-derived wavefront attributes. *Geophysics* 69:265–274
- Fomel S (2011) Theory of 3-D angle gathers in wave-equation seismic imaging. *J Pet Explor Prod Technol* 1:11–16
- Garabito G, Oliva PC, Cruz JCR (2011) Numerical analysis of the finite offset common reflection surface traveltimes approximations. *J Appl Geophys* 74:89–99
- Gelchinsky B, Berkovitch A, Keydar S (1999a) Multifocussing homeomorphic imaging: part 1, basic concepts and formulas. *J Appl Geophys* 42:229–242
- Gelchinsky B, Berkovitch A, Keydar S (1999b) Multifocussing homeomorphic imaging: part 2, multifold data set and multifocussing. *J Appl Geophys* 42:243–260
- Heilmann Z (2007) CRS stack based seismic reflection imaging for land data in time and depth domain. Ph.D. thesis, Karlsruhe University, p 179
- Hertweck T, Schleicher J, Mann J (2007) Data stacking beyond CMP. *Lead Edge* 26(7):818–827
- Höcht G, Ricarte P, Bergler S, Landa E (2009) Operator oriented CRS interpolation. *Geophys Prospect* 57:957–979
- Hubral P (1999) Macro model independent seismic reflection imaging. *J Appl Geophys* 42:137–146
- Mann J (2001) Common reflection surface stack and conflicting dips. In: Extended abstracts, 63rd Conference of European Association of Geoscience Engineering, (Expanded Abstract) Amsterdam, Jun 11–15, p 077
- Mann J (2002) Extensions and applications of the common reflection surface stack method: Ph.D. thesis, University of Karlsruhe, Karlsruhe, p 165
- Mann J, Höcht G, Jäger R, Hubral P (1999) Common reflection surface stack—an attribute analysis. 61st Conference of European Association of Geoscientists and engineers, (Expanded Abstract), Helsinki, Jun 7–11, p 140
- Mann J, Schleicher J, Hertweck T (2007) CRS Stacking; A simplified explanation. EAGE 69th Conference and Technical Exhibition - London, UK
- Müller T (1998) Common reflection surface stack versus NMO/DMO/STACK. 60th Conference of European Association of Geoscientists and engineers, (Expanded Abstract), Leipzig, Jun 8–12, pp 1–20
- Müller T (1999) The common reflection surface stack method: seismic imaging without explicit knowledge of the velocity model. Ph. D. thesis, University of Karlsruhe, Karlsruhe, p 96
- Sajid M, Ghosh DP (2014) Comparative study of new signal processing to improve S/N ratio of seismic data. *J Pet Explor Prod Technol* 4:87–96
- Sava P, Hill SJ (2009) Overview and classification of wavefield seismic imaging methods. *The Leading Edge* 28(2):170–183
- Schwarz B, Vanelle C, Gajewski D, Kashtan B (2014) Curvatures and inhomogeneities: an improved common-reflection-surface approach. *Geophysics* 79(5):231–240
- Shahsavani H, Mann J, Piruz I, Hubral P (2011) A Model based approach to the common diffraction surface Stack. 73rd Conference of European Association of Geoscientists and engineers, (Expanded Abstract), Vienna, May 23–26, p 074
- Soleimani M, Piruz I, Mann J, Hubral P (2009a) Solving the problem of conflicting dips in common reflection surface (CRS) stack. 1st International Petroleum Conference and Exhibition Shiraz, (Extended Abstracts), May 4–6 p A39
- Soleimani M, Piruz I, Mann J, Hubral P (2009b) Common reflection surface stack; accounting for conflicting dip situations by considering all possible dips. *J Seism Explor* 18:271–288
- Spinner M (2007) CRS-based minimum-aperture Kirchho migration in the time domain. Ph. D. thesis, University of Karlsruhe, p 127
- Yang K, Bao-shu Chen BS, Wang XJ, Yang XJ, Liu JR (2012) Handling dip discrimination phenomenon in common reflection surface stack via combination of output imaging scheme and migration/demigration. *Geophys Prospect* 60:255–269